Inorganic Chemistry

Open Access
This article is licensed under CC-BY 4.0

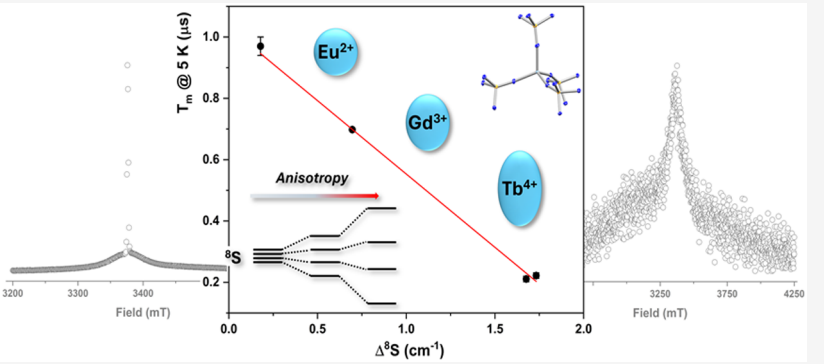
pubs.acs.org/IC
Article

Oxidation State Effects on Decoherence in Isovalent 4f^7 Complexes

Grant R. Wilkinson, Manoj V. H. Subramanya, Maximilian G. Bernbeck, Kavipriya Thangavel, Stephen Hill, and Henry S. La Pierre*

Cite This: *Inorg. Chem.* 2026, 65, 25005−25013
Read Online

ACCESS | Metrics & More | Article Recommendations | Supporting Information



ABSTRACT: The results of pulsed EPR measurements at W-band (94 GHz) on a series of isovalent 4f^7 ions (Eu^{2+}, Gd^{3+}, Tb^{4+}) are presented, constituting the first example to date of pulsed EPR on molecular Tb^{4+}. An inverse correlation is found between the 5 K phase memory relaxation times (T_m) and the degree of zero-field splitting (ZFS) in these complexes. This observation reveals the role of ZFS as an effective reporter not only of structural distortions away from ideal cubic symmetry, but also of the overall electronic structure changes wrought by chemical oxidation, which undermine the seemingly advantageous increases in excited state energies and metal−ligand covalency across the series. Building upon previous studies of the physical properties of high oxidation state lanthanide complexes, these results further highlight the necessity for detailed electronic structure−property relationship studies to fully map the electronic consequences of chemical oxidation in the lanthanides.

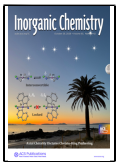
INTRODUCTION

Among molecular complexes of lanthanide ions, Gd^{3+} has demonstrated excellent potential for applications in the design of molecular spin qubits owing to its chemical stability and isotropic valence electron configuration.[1−9] The 4f^7 configuration of Gd^{3+} possesses zero orbital angular momentum (and thus first-order spin−orbit coupling is inoperable) and, in general, such isotropic electronic states demonstrate insensitivity to coupled vibrational modes, thus increasing both spin−lattice (T_1) and phase memory (T_m) coherence times (in T_1 limited regimes).[5,10−12] Despite the advantageous benefits of the 4f^7 configuration for Gd^{3+}, there has been minimal to no extension to the isoelectronic congeners Eu^{2+} and Tb^{4+} in the context of quantum information science.

Though both ions are accessible under the appropriate conditions, the disparate requirements for stabilization of Eu^{2+} and Tb^{4+} in molecular species have precluded detailed studies of the effects of chemical oxidation in an isoelectronic 4f^7 series on fundamental electronic structure and decoherence properties. This issue is particularly pronounced for Tb^{4+}, and high-oxidation state non-Ce^{4+} lanthanide ions in general, where isolable molecular complexes have only been available since 2019, with only a handful of ligand frameworks demonstrating suitable stabilization of these ions to enable detailed physical characterization.[13−26] The physical properties thus far elucidated for these ions point to distinct changes in fundamental electronic structure as a function of oxidation state, with increases in metal−ligand covalency and crystal field interactions leading to significant perturbation of the free-ion contributions.[27]

For Pr^{4+}, recent work in extended solids[28−31] and molecular complexes[19,21] demonstrates how the increase in crystal field splitting leads to competition with spin−orbit coupling. This intermediate coupling regime quenches the orbital angular momentum, affording a greater isotropic character for the ion and enhancing its coherence properties.[29,30] In contrast, the formally isotropic Tb^{4+} gains anisotropy through mixing of excited states into the ground $^8S_{7/2}$ state facilitated by second-order spin−orbit coupling and intra-ion spin−spin cou-

Received: August 6, 2026
Revised: September 25, 2026
Accepted: September 30, 2026
Published: October 8, 2026



ACS Publications
© 2026 The Authors. Published by American Chemical Society

https://doi.org/10.1021/acs.inorgchem.6c04187
Inorg. Chem. 2026, 65, 25005−25013

Downloaded from pubs.acs.org/inocaj/article-pdf/65/42/25005/6793688/acs.inorgchem.6c04187.pdf by FLORIDA STATE UNIV user on 02 November 2026

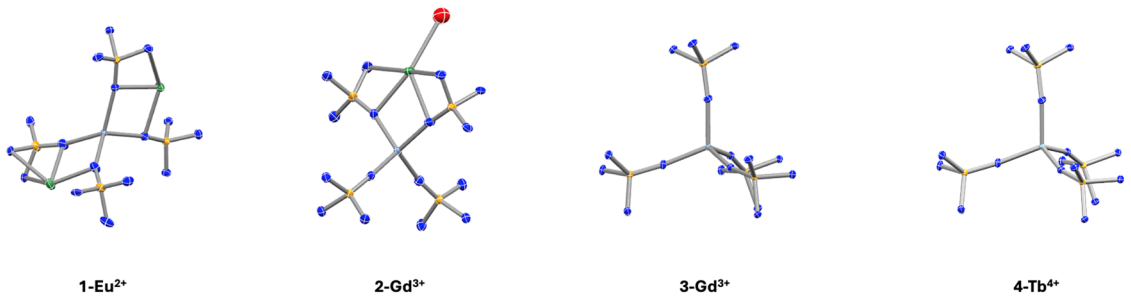


Figure 1. Molecular structures of **1-Eu**$^{2+}$, **2-Gd**$^{3+}$, **3-Gd**$^{3+}$, and **4-Tb**$^{4+}$ with thermal ellipsoids set at 50%. Cyan, blue, orange, red, and green represent the lanthanide atom, nitrogen, phosphorus, oxygen, and potassium, respectively. All carbon and hydrogen atoms, along with disordered components and noncoordinated solvents are omitted for clarity.

pling.[32,33] This phenomenon is parametrized by the zero-field splitting (ZFS) of the ground octet.

To investigate how modulation of the underlying electronic structure as a function of oxidation state directs ZFS, our group previously reported the only extant series of molecular Eu^{2+}, Gd^{3+}, and Tb^{4+} ions in a mostly conserved coordination environment.[34] In this series, where each ion is supported by four [NP(1,2-bis-^{t}Bu-diamidoethane)(NEt_2)]$^-$ ([NP*]$^-$) imidophosphorane ligands (Figures 1 and 2), high-frequency/

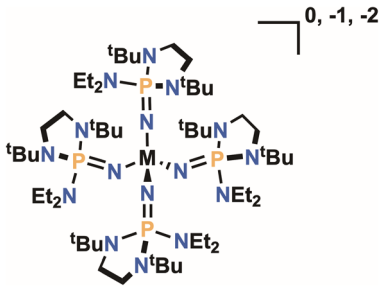


Figure 2. Representative molecular structure of a [M(NP(1,2-bis-^{t}Bu-diamidoethane)NEt_2)$_4$] complex where M = Eu^{2+}, Gd^{3+}, or Tb^{4+}.

high-field continuous-wave (CW) EPR and complementary theoretical calculations were performed to examine the static electronic properties of these complexes.[34] In these studies, it was found that ZFS increased moving from Eu^{2+} to Gd^{3+} to Tb^{4+}, driven primarily by the increase in second-order spin orbit coupling,[34] with the increasing spin−orbit coupling constant, ζ, consistent with the increased effective nuclear charge both across the series and with increasing oxidation state.[35] This occurs despite the increasing energy gap between the ground ^{8}S and excited ^{6}P state across the series,[34] which should reduce the degree of state mixing, holding other contributions constant.

Additionally, the increasing magnitude of the crystal field and metal−ligand bond covalency as a function of increasing oxidation state in these ions serves to magnify the effects of structural distortions away from ideal T_d symmetry, where ZFS is quenched.[32,33] This greater crystal field strength results in an increase in the overall splitting of the excited ^{6}P state, lowering the effective energy gap to the ground state and further enabling state mixing giving rise to anisotropy.

The impact of the individual components of an ion's electronic structure on the relaxation properties of qubits has been well studied in transition metals.[36−51] While several studies have sought to establish optimal criteria for qubits based upon the tuning of one or more of these parameters, competition between individual perturbations has hindered their development and represents a critical tension in the design of molecular spin qubits. For these $4f^7$ ions, this interplay drives their sensitivity to static structural distortions giving rise to anisotropy, which in turn enhances spin−lattice relaxation,[5] the main driver of T_m at high temperatures. To further understand the competition between these phenomena in formally isotropic $4f^7$ ions, the resulting coherence properties, and the underlying electronic structure of these ions, we present pulsed electron paramagnetic resonance (EPR) spectroscopy data of an isoelectronic (f^7), isovalent series of Eu^{2+}, Gd^{3+}, and Tb^{4+} complexes. These data constitute the first example to date of such experiments reported for molecular Tb^{4+} and establish a correlation between enhanced environmental sensitivity as a function of increased oxidation state and coherence lifetime of the central transition in the only three available ions bearing the $4f^7$ valence configuration.

RESULTS

Synthesis and Structure

The analytes [(Et_2O)K][Gd(NP*)$_4$] (**2-Gd**$^{3+}$), [(2.2.2-crypt)-K][Gd(NP*)$_4$] (**3-Gd**$^{3+}$) and [Tb(NP*)$_4$] (**4-Tb**$^{4+}$) (Figure 2) were synthesized as previously described while [K_2Eu-(NP*)$_4$] (**1-Eu**$^{2+}$) was synthesized through a modification of the procedure for [(THF)K][(Et_2O)K][Eu(NP*)$_4$].[14,34] The deviation from ideal T_d symmetry for the first coordination sphere of these complexes was quantified using the $\Sigma_{109.5}$ metric, which reports the sum of deviations of the six angles of a four-coordinate complex from the ideal 109.5° tetrahedral angle.[52] Complexes **2-Gd**$^{3+}$, **3-Gd**$^{3+}$, and **4-Tb**$^{4+}$ have $\Sigma_{109.5}$ values of 28.4, 6.0, and 9.8° respectively,[34] and **1-Eu**$^{2+}$ was found to have a value of 64.7°. Detailed structural comparisons of **1-Eu**$^{2+}$ and the previously reported [(THF)K][(Et_2O)K]-[Eu(NP*)$_4$] can be found in the Supporting Information. Truncated molecular structures for the compounds investigated in this study are shown in Figure 1.

Pulsed EPR Spectroscopy

Pulsed W-band (94 GHz) EPR measurements were performed using the high-power quasi-optical W-band spectrometer (HiPER) located at the National High Magnetic Field Laboratory (NHMFL) in Tallahassee, Florida[53,54] on 2 mM frozen solutions of the analytes in either toluene (**1-Eu**$^{2+}$, **2-Gd**$^{3+}$, **4-Tb**$^{4+}_{tol}$) or 2-methyltetrahydrofuran (2-MeTHF) (**3-Gd**$^{3+}$, **4-Tb**$^{4+}_{THF}$). Further details regarding the spectrometer configuration and sample preparation can be found in the Supporting Information.

Downloaded from pubs.acs.org/inoaj/article-pdf/65/42/25005/6793688/acs.inorgchem.6c04187.pdf by FLORIDA STATE UNIV user on 02 November 2026

https://doi.org/10.1021/acs.inorgchem.6c04187
Inorg. Chem. 2026, 65, 25005−25013

Echo-Detected Field-Swept Spectra

Echo-detected field-swept (EDFS) spectra were collected for each sample at 5 K using a standard two-pulse Hahn echo sequence $(\pi/2 - \tau - \pi - \tau - echo)$. Pulse lengths and wait times were varied to optimize echo intensity for each sample. Spectra were fit in *EasySpin*[55] using the effective spin-7/2 Hamiltonian

$$\hat{H}_{spin} = g_{iso}\mu_B \vec{B}\cdot\hat{S} + D\left\{\hat{S}_z^{\,2} - \frac{1}{3}S(S+1)\right\} + E(\hat{S}_x^{\,2} - \hat{S}_y^{\,2}) \quad (1)$$

where g_{iso} is the isotropic g-value, μ_B the Bohr magneton, $\vec{B}$ the magnetic field vector, $\hat{S}$ the electronic spin operator, S the total spin of the system ($S = 7/2$), $\hat{S}_i$ ($i = x,y,z$) the components of the electronic spin operator along the x, y, and z directions respectively, and D and E the axial and rhombic components of the ZFS interaction. Results of the fits are given in Table 1, and the experimental spectra and fine-point simulations for **3-Gd^{3+}** and **4-Tb$^{4+}_{THF}$** are plotted in Figure 3.

Table 1. Spin Hamiltonian Fit Parameters and Δ^8S Values

Sample	g_{iso}	D (cm^{-1})	E (cm^{-1})	Δ^8S (cm^{-1})
1-Eu^{2+}	1.9872(3)	−0.05043(13)	−0.0135(2)	0.696
2-Gd^{3+}	1.9878(6)	0.0807(2)	0.02178(14)	1.115
3-Gd^{3+}	1.9891(6)	0.0123(6)	0.0041(6)	0.179
4-Tb$^{4+}_{tol}$	2.0021(6)	0.1232(5)	0.0362(4)	1.733
4-Tb$^{4+}_{THF}$	2.0005(8)	0.1160(9)	0.0383(5)	1.676

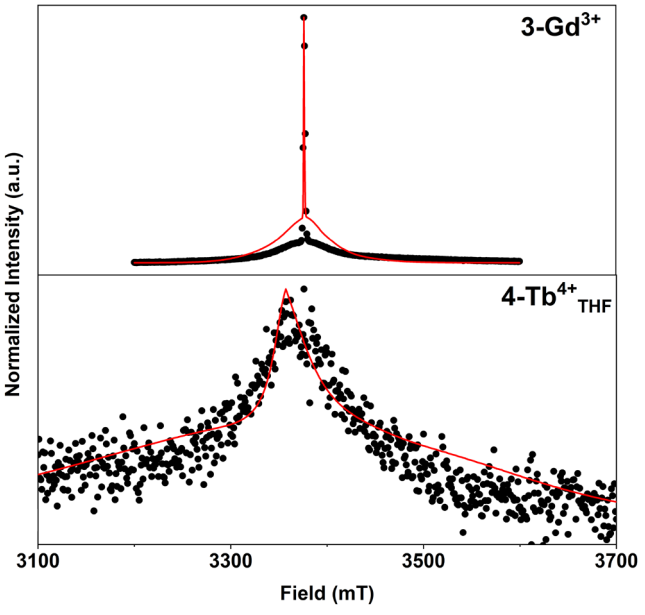


Figure 3. Co-plot of EDFS data (black) and fine-point simulations (red) for **3-Gd^{3+}** and **4-Tb$^{4+}_{THF}$** in the range 3100−3700 mT at 5 K.

Anisotropic line broadening was introduced as strain in the ZFS parameters (σ_D and σ_E), with both parameters fixed to their reported values[34] (those of [(THF)K][(Et$_2$O)K][Eu(NP*)$_4$] used for **1-Eu^{2+}**) and modeled using explicit averaging. To minimize computational resources needed for fitting, the spectra were initially fit using a coarse sampling of the strain distributions (Figures S7−S11) and final simulations using the stable fit parameters were performed with finer samples to minimize truncation artifacts (Figures S12−S16, see Supporting Information for full fitting details). The energetic separation between the highest and lowest m_s doublets of the ground ^{8}S state in absence of an applied field, denoted Δ^8S,[34] is calculated as the range of the eigenvalues of the ZFS operator and is given for each sample in Table 1.

T_1 and T_m Measurements. Variable-temperature T_1 and T_m measurements were performed at the field of maximum echo intensity corresponding to the central $m_s = -1/2 \rightarrow m_s = 1/2$ transition for each analyte. Standard inversion recovery ($\pi - t_{wait} - \pi/2 - \tau - \pi - \tau - echo$) and two-pulse Hahn echo ($\pi/2 - \tau - \pi - \tau - echo$) sequences were used to measure T_1 and T_m, respectively, at each temperature. Pulse parameters were optimized for each temperature and sample to maximize echo intensity. Standard monoexponential functions were used to extract T_1 and T_m (see Supporting Information for full details). Each measurement was performed in at least duplicate, and the presented results are arithmetic averages of the relevant data points with errors calculated via Gaussian error propagation. Full results are presented in Tables S4 and S5 and low-temperature results for **3-Gd^{3+}** and **4-Tb$^{4+}_{THF}$** are plotted in Figure 4 (See Figures S18−S22 for full results).

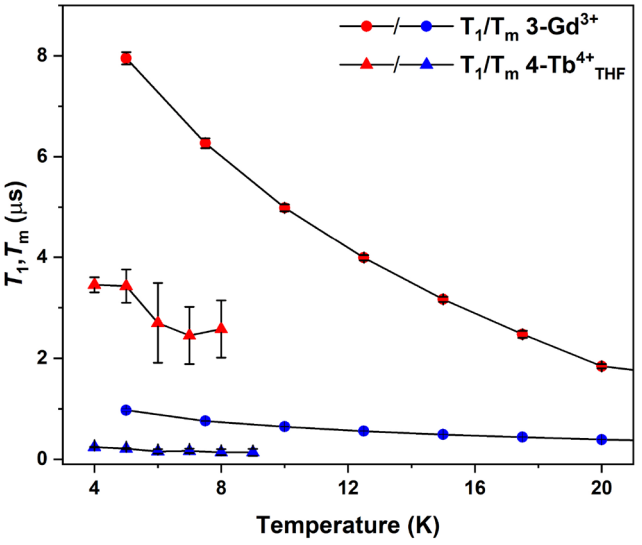


Figure 4. Co-plot of low-temperature T_1 (red) and T_m (blue) vs temperature results for **3-Gd^{3+}** (circles) and **4-Tb$^{4+}_{THF}$** (triangles). Lines between data points serve as visual guides.

Measurements were performed at increasing temperatures until echoes were sufficiently weak to preclude meaningful interpretation. Additional data points were collected at temperatures below 5 K for the **4-Tb^{4+}** species to supplement the small number of data points acquired at higher temperatures for these samples. Log−log plots of $1/T_1$ vs temperature are given in Figures S23−S27, and fits of the observed linear regimes reveal temperature dependencies for $1/T_1$ ranging $T^{0.40}$-$T^{2.01}$ across all samples.

T_m Fittings. Fitting of the T_m data for **1-Eu^{2+}**, **2-Gd^{3+}**, and **3-Gd^{3+}** were performed using a modified version of the coherence lifetime model for the central transition proposed by Wilson et al.[56]

$$\frac{1}{T_m} = A_1\omega_{dd}(\bar{r}) \sum_{m,m'} W_{m,m'}n_m n_{m'} + \frac{F}{T_1} \quad (2)$$

Downloaded from pubs.acs.org/inoaaj/article-pdf/65/42/25005/6793688/acs.inorgchem.6c04187.pdf by FLORIDA STATE UNIV user on 02 November 2026

https://doi.org/10.1021/acs.inorgchem.6c04187
Inorg. Chem. 2026, 65, 25005−25013

where A_1 and F weight the individual contributions, $\omega_{dd}(\bar{r})$ is the dipole−dipole coupling strength for neighboring spin centers at an average distance $\bar{r}$, $W_{m,m'}$ is the overlap matrix element for an energy-conserving spin flip-flop between neighboring spin centers in arbitrary spin projection states m and m' weighted by their respective Boltzmann populations n_m and $n_{m'}$, and T_1 is the spin−lattice relaxation time. Details on the full derivation of this modified model can be found in the Supporting Information. Fit results are summarized in Table 2

Table 2. Results of Equation 2 Fits and Experimental, Full Fit, and Linear Extrapolation Values for $1/T_m$ at 5 K for 1-Eu^{2+}, 2-Gd^{3+}, and 3-Gd^{3+}

Sample	$A_1(10^{-3})$	F	$1/T_m$, Experimental 5 K (μs^{-1})	$1/T_m$, Full Fit 5 K (μs^{-1})	$1/T_m$, Extrapolated 5 K (μs^{-1})
1-Eu^{2+}	5.0(8)	1.7(2)	1.433(11)	1.63	3.18
2-Gd^{3+}	1.2(6)	3.74(17)	1.117(15)	1.23	1.63
3-Gd^{3+}	2.7(4)	2.47(10)	1.03(3)	0.76	1.65

and full fit results are given in Figures S28−S30. The 5 K values for $1/T_m$ obtained experimentally and from the full fit in eq 2 are given in Table 2. The corresponding values obtained from extrapolating the high-temperature linear regime to 5 K (Figures S31−S33) are also provided.

DISCUSSION

The analytes of interest in this study were synthesized as previously described,[14,34] except in the case of **1-Eu^{2+}**, which necessitated a slight modification of the reported procedure to preclude coordinating solvents.[34] The fit parameters for the EDFS spectra collected for each sample at 5 K are in reasonable agreement (as applicable) with those previously reported for solid-state and solution phase measurements.[34] All spectra (Figures S7−S16) display broad features over much of the spectral width as a consequence of the large strain in ZFS parameters,[32] which broadens many of the available transitions, as observed in the previous CW study.[34] Additionally, a relatively sharp peak around $g = 2$ corresponding to the central transition is observed in all spectra.

To look for any trends in relaxation times across the series, variable-temperature T_1 and T_m measurements were performed for each analyte. Qualitatively, a clear trend of increasing T_1 and T_m for a given temperature appears upon moving from **1-Eu^{2+}** to **2-Gd^{3+}** to **3-Gd^{3+}** (Figures S18−S22). This trend mirrors the increase in the excited ^6P state energy moving from Eu^{2+} to Gd^{3+} and the decrease in distortion from T_d quantified by the decreasing $\Sigma_{109.5}$ values (**1-Eu^{2+}**: 64.7°, **2-Gd^{3+}**: 28.4°, **3-Gd^{3+}**: 6.0°),[34] with the increase from **2-Gd^{3+}** to **3-Gd^{3+}** accounted for by the decrease in distortion away from ideal T_d symmetry moving from an inner-sphere to an outer-sphere potassium cation. Based on this initial behavior, one might expect that the **4-Tb^{4+}** species, with an even higher ^6P energy and a similarly small distortion from T_d ($\Sigma_{109.5}$: 9.8°)[34] as **3-Gd^{3+}**, to follow this apparent trend. The opposite, however, is observed, with clear decreases from the Gd^{3+} species in both T_1 and T_m. In fact, **4-Tb^{4+}_{tol}** and **4-Tb^{4+}_{THF}** display the shortest T_m times across the entire series with exceptionally weak signal-to-noise ratios, even at 5 K, and large relative errors in T_1 values. Decreasing relaxation times upon moving from Gd^{3+} to Tb^{4+} are not without precedent, with reports from both extended-solid and molecular species of greater thermal attenuation of CW EPR signals for Tb^{4+} systems indicative of shorter T_1 times. To the best of our knowledge, no studies have elucidated the physical basis for this phenomenon.

To understand the mechanisms driving T_1, the linear regimes of log−log plots of $1/T_1$ vs temperature were fit for each analyte (Figures S23−S27), revealing temperature dependencies for the spin−lattice relaxation rate spanning $T^{0.40}$-$T^{2.01}$. These results suggest that relaxation is primarily driven by direct processes in all compounds, with some higher order processes (such as Raman or Orbach) gaining prominence at higher temperature.[42,57−59] The dominance of direct processes is not unexpected given the B^4 dependence of this mechanism[58] and the high magnetic fields (~3.35 T) at which the experiments were conducted. Given the T_1 enhancements noted for isotropic systems,[5,10−12] it is expected that T_1 should scale inversely with increasing anisotropy (ZFS) holding other contributions constant. Despite this, no clear correlation is observed between the measured low temperature T_1 (5 K) values and the total splitting of the ground ^8S state at zero-field, denoted Δ^8S (Figure S34), chosen to minimize ambiguities in comparing multiple ZFS terms of opposite sign. Confounding factors include differential coupling strengths to molecular vibrations, an active area of computational development.[48,60−64]

Considering T_m values, the coherence lifetime model proposed by Wilson et al. for the central transition provides an excellent starting point.[56] This model explicitly considers three contributions to decoherence: (1) energy conserving nearest-neighbor electron spin flip-flops, (2) direct T_1-driven decoherence, and (3) T_1-induced relaxation on neighboring spins. At low temperature, T_1 contributions should be minimal, allowing for examination of how electronic structure changes affect the contribution of the electron flip-flop mechanism, alongside other effects, such as nuclear spin diffusion and methyl tunnelling, that are not explicitly treated in this model.[42,56]

Interestingly, an inverse correlation is found between the 5 K T_m values and Δ^8S for these compounds (Figure 5). While this correlation might be consistent with T_1-driven decoherence (mechanisms 2 and 3 in the Wilson model), as ZFS induced anisotropy is expected to shorten T_1, no correlation can be

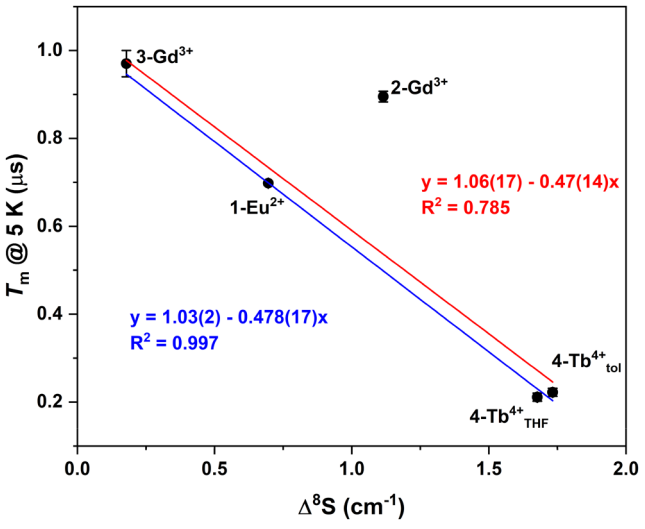


Figure 5. Plot of T_m values at 5 K vs Δ^8S. Linear fits of the data are shown considering (red) and neglecting (blue) the **2-Gd^{3+}** result.

https://doi.org/10.1021/acs.inorgchem.6c04187
Inorg. Chem. 2026, 65, 25005−25013

Downloaded from pubs.acs.org/inocaj/article-pdf/65/42/25005/6793688/acs.inorgchem.6c04187.pdf by FLORIDA STATE UNIV user on 02 November 2026

found between T_m and T_1 at 5 K (Figure S37). To further examine the physical basis for this correlation, a modified form of Wilson's model (eq 2) was employed, where mechanisms 2 and 3, which both depend on T_1, are treated as a single component weighted by F. This simplification was necessitated by the lack of variable concentration data needed to differentiate contributions from the two mechanisms. Sufficient data were available for **1-Eu^{2+}**, **2-Gd^{3+}**, and **3-Gd^{3+}** to apply this truncated model to these data sets and results are presented in Table 2 and Figures S28−S30. Attempts were made to apply this model to the **4-Tb$^{4+}_{tol}$** and **4-Tb$^{4+}_{THF}$** data sets, but the small number of data points combined with the large errors in T_1 and T_m present in both precluded meaningful fits.

Considering the individual fits, a clear difference between the results for **1-Eu^{2+}** and **3-Gd^{3+}** vs those of **2-Gd^{3+}** can be seen at lower temperatures, where **1-Eu^{2+}** and **3-Gd^{3+}** demonstrate a deviation from linearity with decreasing temperature that is absent in **2-Gd^{3+}** (Figure 6). The observed

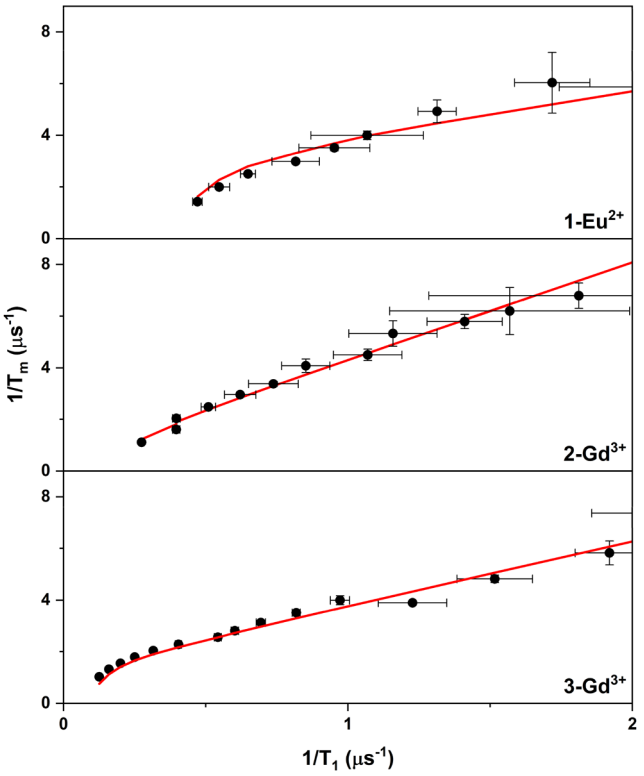


Figure 6. Low temperature plot of $1/T_m$ vs $1/T_1$ for **1-Eu^{2+}** (top, ≤ 22.5 K) **2-Gd^{3+}** (middle, ≤ 35 K), and **3-Gd^{3+}** (bottom, ≤ 45 K) with associated errors. Fits of eq 2 to the data are shown in red.

deviation from linearity with respect to $1/T_1$ in **1-Eu^{2+}** and **3-Gd^{3+}** is consistent with mechanism (1) from the Wilson model dominating relaxation at low temperatures, as anticipated, while the absence of this deviation in **2-Gd^{3+}** is suggestive of T_1 driven processes being more important at low temperatures in this system. This interpretation is consistent with the results of the fits to eq 2, which reveal a smaller A_1 and larger F value for **2-Gd^{3+}** than those found for the other compounds. Further evidence of the stronger influence of T_1 contributions on the low temperature decoherence of **2-Gd^{3+}** can be found through extrapolation of the high-temperature linear, T_1-limited regimes of each data set to low temperature (Figures S31−S33). The resulting $1/T_m$ values predicted by the full fit and the extrapolation are presented in Table 2 alongside the experimental values.

Notably, the extrapolated $1/T_m$ values for **1-Eu^{2+}** and **3-Gd^{3+}** overestimate the decoherence rate roughly 2-fold as compared to the full fit values, while **2-Gd^{3+}** demonstrates a greater agreement between the two values, with only a 33% overestimation from the extrapolation of the high-temperature behavior. A similar observation can be made comparing the extrapolated values to the experimental data points, though the overestimation in **3-Gd^{3+}** in this comparison is somewhat attenuated with respect to the full fit values. This analysis supports the classification of **2-Gd^{3+}**, which deviates from the linear correlation between T_m at 5 K and Δ^8S observed for the other compounds, as an outlier. The physical basis for this outlier behavior is not immediately apparent from this analysis, however the presence of a pendant diethyl ether, which has several noted low energy (∼100 cm^{-1}) vibrational modes[65,66] available for coupling to the metal center and is absent in the other complexes, may contribute to the extension of the T_1-driven regime to lower temperatures in **2-Gd^{3+}**. Detailed low energy IR and/or Raman experiments coupled with theoretical calculations may shed further light on this behavior but are beyond the scope of this report.

Regardless, exclusion of the **2-Gd^{3+}** data point from the linear fit then results in a near perfect inverse correlation between the two parameters, as evidenced by the near unity R^2 value (Figure 5). It is important to note that this empirical linear relationship should be interpreted with caution as, for values of Δ^8S greater than 2.15 cm^{-1}, this relationship cannot be valid as it predicts unphysically negative T_m values, suggesting additional parameters or higher-order functional forms are necessary to describe the relationship between Δ^8S and T_m in these cases.

To better understand the source of this correlation, the Wilson model is examined in more detail. From the original model, the A_1 term, which represents the contribution of the energy-conserving spin flip-flop mechanism to decoherence, is expected to scale inversely with the EPR line width. Wilson et al. proxy the line width with the degree of ZFS,[56] which applied to the compounds in this study, would imply a larger A_1 term for **1-Eu^{2+}** than **3-Gd^{3+}**, the opposite of the observed behavior. This highlights a potential deficiency in the model to accurately weight the disparate broadenings of the m_s sublevels by the ZFS,[56] though the influence of additional extrinsic factors (i.e., disorder or unresolved hyperfine coupling) on the phenomenological line widths cannot be discounted. Additionally, other processes which may be critical to decoherence in these systems, such as nuclear spin flip-flops,[42] are not explicitly accounted for in the original model, and likely contribute at low temperatures.

This abridged model still leaves unclear, however, why the ZFS, which classically describes only the anisotropy of the ion and thus should primarily drive changes in T_1 behavior,[5,10−12] should correlate with T_m. While the ZFS in these systems is primarily driven by second-order spin−orbit coupling, it ultimately represents an aggregate of the electronic and structural perturbations present in this system that promote mixing of excited states into the ground state, which may in turn serve to shorten T_m. The rapid relaxation of the **4-Tb^{4+}** species, however, obfuscates detailed interpretation, necessitating further synthetic design to achieve a molecular Tb^{4+} species with sufficiently long T_1 and T_m times at low temperature to

Downloaded from pubs.acs.org/inoaj/article-pdf/65/42/25005/6793688/acs.inorgchem.6c04187.pdf by FLORIDA STATE UNIV user on 02 November 2026

https://doi.org/10.1021/acs.inorgchem.6c04187
Inorg. Chem. 2026, 65, 25005−25013

enable Wilson analyses. Therefore, elucidation of the basis for this observed correlation will entail further studies of new, carefully designed $4f^7$ series, paired with appropriate theoretical modeling. Examination of the concentration-dependence of the decoherence behavior will be particularly illuminating, enabling fitting with the full Wilson model to determine the limiting dipole−dipole interaction distance between neighboring electron spin centers.[56] Additionally, rigorously isostructural analytes across all three isoelectronic ions would enable disambiguation of the role of structural and electronic contributions to the ZFS, and thus the decoherence properties of these ions.

As previously alluded, studies of isotropic metal ions (including Gd^{3+}) have clearly demonstrated the diminished sensitivity of T_1 and T_m to vibrations due to a lack of orbital anisotropy.[5,10−12] While the formally isotropic $4f^7$ configuration of the ions studied here should afford the same benefits in the absence of first-order orbital angular momentum, the observed trends in ZFS and 5 K T_m suggest that subtle changes in overall electronic structure within this series, as reported by the aggregate Δ^8S term, drive enhanced decoherence as a function of chemical oxidation state, despite seemingly advantageous changes in individual perturbations.

CONCLUSIONS

In this work, we present W-band pulsed EPR measurements on an isovalent series of Eu^{2+}, Gd^{3+}, and Tb^{4+} complexes. Though no clear correlation was observed between T_1 at 5 K and the zero-field splitting of the ^8S ground state (Δ^8S), an inverse correlation between the T_m value at 5 K and Δ^8S is observed. This result emphasizes how tuning of the electronic structure in formally isotropic ions via chemical oxidation can undermine quantum coherence and highlights the need for concentration-dependent studies and rigorously isostructural analytes to fully map these effects. Though limited to the only available molecular series of Eu^{2+}, Gd^{3+}, and Tb^{4+} ions, this work more broadly demonstrates the disparities in electronic structure and resulting properties between differing oxidation states in lanthanide ions. These results also highlight the necessity of rigorously cubic coordination environments to realize Tb^{4+} qubits through the quenching of ZFS perturbations. The observed sensitivity of coherence properties to perturbations additionally commends dynamic EPR studies to map the effects of bonding in $5f^7$ ions (Cm^{3+} and Bk^{4+}) wherein ligand-5f orbital overlap further increases crystal field and covalency contributions.

EXPERIMENTAL SECTION

Synthetic details for **1-Eu^{2+}** are given here. General considerations, characterization details, including IR spectroscopy, DC magnetometry, and crystallography, and details on pulsed EPR spectroscopy measurement, data processing and fitting are provided in the SI.

$[K_2Eu(NP^*)_4]$ (1-Eu^{2+})

This compound was synthesized following a modified literature procedure. In the glovebox, a 20 mL scintillation vial was charged with $[EuI_2(THF)_2]$ (105.85 mg, 0.191 mmol), hexanes (2 mL), and a glass coated magnetic stirring bar. To this mixture was added a solution of $[K(NP(CH_2N^tBu)_2(Et_2N))]$ (249.78 mg, 0.765 mmol, 4.01 equiv) in hexanes (2 mL), and the resulting light green suspension was allowed to stir overnight at room temperature. The now bright orange reaction mixture was filtered through a pad of Celite on a fine porosity glass frit, and the tan solids were washed with minimal additional hexanes. The resulting bright orange filtrate was reduced *in vacuo* and triturated with pentane (3 × 2 mL) to afford a waxy orange residue. This residue was crystallized from evaporation of a concentrated solution in pentane into a reservoir of toluene at −35 °C to afford the product as XRD quality single crystals (187.06 mg, 71%). IR (cm^{-1}): *v.* 3015 (vw), 2964 (w), 2902 (w), 2829 (w), 1463 (vw), 1384 (w), 1355 (w), 1305 (vw), 1262 (w), 1245 (w), 1196 (s), 1178 (s), 1143 (m), 1093 (vw), 1040 (m), 1021 (m), 966 (m), 917 (m), 863 (w), 789 (w), 679 (s), 608 (w), 517 (w), 492 (s), 465 (w), 447 (vw). Elem. Anal. Found (calc): C, 48.60 (48.75); H, 9.46 (9.35); N, 16.20 (16.24).

ASSOCIATED CONTENT

Supporting Information

The Supporting Information is available free of charge at https://pubs.acs.org/doi/10.1021/acs.inorgchem.6c04187.

General considerations, IR and EPR spectroscopy, magnetometry, and crystallographic data (PDF)

Accession Codes

Deposition Number 2473801 contains the supplementary crystallographic data for this paper. These data can be obtained free of charge via the joint Cambridge Crystallographic Data Centre (CCDC) and Fachinformationszentrum Karlsruhe Access Structures service.

AUTHOR INFORMATION

Corresponding Author

Henry S. La Pierre − *School of Chemistry and Biochemistry, Georgia Institute of Technology, Atlanta, Georgia 30332-0400, United States; Nuclear and Radiological Engineering and Medical Physics Program, School of Mechanical Engineering, Georgia Institute of Technology, Atlanta, Georgia 30332-0400, United States; Physical Sciences Division, Pacific Northwest National Laboratory, Richland, Washington 99352, United States;* orcid.org/0000-0002-0895-0655; Email: hsl@gatech.edu

Authors

Grant R. Wilkinson − *School of Chemistry and Biochemistry, Georgia Institute of Technology, Atlanta, Georgia 30332-0400, United States;* orcid.org/0000-0001-9701-3016

Manoj V. H. Subramanya − *National High Magnetic Field Laboratory, Florida State University, Tallahassee, Florida 32310, United States;* orcid.org/0009-0000-4032-5852

Maximilian G. Bernbeck − *School of Chemistry and Biochemistry, Georgia Institute of Technology, Atlanta, Georgia 30332-0400, United States;* orcid.org/0000-0001-6329-5860

Kavipriya Thangavel − *National High Magnetic Field Laboratory, Florida State University, Tallahassee, Florida 32310, United States*

Stephen Hill − *National High Magnetic Field Laboratory, Florida State University, Tallahassee, Florida 32310, United States; Department of Physics and Department of Chemistry and Biochemistry, Florida State University, Tallahassee, Florida 32306, United States;* orcid.org/0000-0001-6742-3620

Complete contact information is available at: https://pubs.acs.org/10.1021/acs.inorgchem.6c04187

Notes

The authors declare no competing financial interest.

https://doi.org/10.1021/acs.inorgchem.6c04187
Inorg. Chem. 2026, 65, 25005−25013

Downloaded from pubs.acs.org/inoca/article-pdf/65/42/25005/6793688/acs.inorgchem.6c04187.pdf by FLORIDA STATE UNIV user on 02 November 2026

■ ACKNOWLEDGMENTS

We thank Prof. C. Blake Wilson (University of Southern California) for helpful discussions regarding the application of the high-field coherence lifetime model. These studies were supported by the U.S. Department of Energy, Office of Science, Basic Energy Sciences, Quantum Information Science initiative under Grant No. DE-SC0023455 (M.G.B., H.S.L.). H.S.L. is an Alfred P. Sloan Research Fellow. G.R.W. was supported by the National Science Foundation Graduate Research Fellowship under Grant No. DGE-2039655. Any opinions, findings, and conclusions or recommendations expressed in this material are those of the author(s) and do not necessarily reflect the views of the National Science Foundation. M.V.H.S. was supported by the Office of Naval Research under Grant No. N62909-23-1-2079. The National High Magnetic Field Laboratory is supported by the National Science Foundation through NSF/DMR-2128556 and the State of Florida.

■ REFERENCES

(1) Martínez-Pérez, M. J.; Cardona-Serra, S.; Schlegel, C.; Moro, F.; Alonso, P. J.; Prima-García, H.; Clemente-Juan, J. M.; Evangelisti, M.; Gaita-Ariño, A.; Sesé, J.; Van Slageren, J.; Coronado, E.; Luis, F. Gd-Based Single-Ion Magnets with Tunable Magnetic Anisotropy: Molecular Design of Spin Qubits. *Phys. Rev. Lett.* **2012**, *108* (24), No. 247213, DOI: 10.1103/PhysRevLett.108.247213.

(2) Jenkins, M. D.; Duan, Y.; Diosdado, B.; García-Ripoll, J. J.; Gaita-Ariño, A.; Giménez-Saiz, C.; Alonso, P. J.; Coronado, E.; Luis, F. Coherent manipulation of three-qubit states in a molecular single-ion magnet. *Phys. Rev. B* **2017**, *95* (6), No. 064423, DOI: 10.1103/PhysRevB.95.064423.

(3) Handzlik, G.; Magott, M.; Arczyński, M.; Sheveleva, A. M.; Tuna, F.; Sarewicz, M.; Osyczka, A.; Rams, M.; Vieru, V.; Chibotaru, L. F.; Pinkowicz, D. Magnetization Dynamics and Coherent Spin Manipulation of a Propeller Gd(III) Complex with the Smallest Helicene Ligand. *J. Phys. Chem. Lett.* **2020**, *11* (4), 1508−1515.

(4) López-Cabrelles, J.; Escalera-Moreno, L.; Hu, Z.; Prima-García, H.; Espallargas, G. M.; Gaita-Ariño, A.; Coronado, E. Near Isotropic D_{4d} Spin Qubits as Nodes of a Gd(III)-Based Metal−Organic Framework. *Inorg. Chem.* **2021**, *60* (12), 8575−8580.

(5) Buch, C. D.; Kundu, K.; Marbey, J. J.; Van Tol, J.; Weihe, H.; Hill, S.; Piligkos, S. Spin−Lattice Relaxation Decoherence Suppression in Vanishing Orbital Angular Momentum Qubits. *J. Am. Chem. Soc.* **2022**, *144* (38), 17597−17603.

(6) Wang, J.; Jing, Y.; Cui, M. H.; Lu, Y. M.; Ouyang, Z.; Shao, C.; Wang, Z.; Song, Y. Spin Qubit in a 2D $Gd^{III}Na^{I}$-Based Oxamato Supramolecular Coordination Framework. *Chem.-Eur. J.* **2023**, *29* (66), No. e202301771, DOI: 10.1002/chem.202301771.

(7) Hansen, S. H.; Buch, C. D.; Petersen, J. B.; Rix, M.; Ubach I Cervera, M.; Strandfelt, A.; Winpenny, R. E. P.; McInnes, E. J. L.; Piligkos, S. Probing decoherence in molecular 4f qubits. *Chem. Sci.* **2024**, *15* (48), 20328−20337.

(8) Hansen, S. H.; Buch, C. D.; Weihe, H.; Piligkos, S. Effect of Chemical Modification in Trigonal Gd(III) Molecular Qubits. *Inorg. Chem.* **2025**, *64* (10), 4912−4919.

(9) Rodríguez-Esteban, C.; Ruiz-Bilbao, E.; Bustamante-Fernández, J.; Tuna, F.; Lezama, L.; Mailman, A.; Ullah, A.; Gaita-Ariño, A.; Artetxe, B.; Gonidec, M.; Oyarzabal, I. Coherent Spin Manipulation in Mononuclear Gadolinium-Substituted Polyoxometalate−Organic Hybrids. *J. Phys. Chem. Lett.* **2025**, *16* (12), 3072−3077.

(10) Ariciu, A.-M.; Woen, D. H.; Huh, D. N.; Nodaraki, L. E.; Kostopoulos, A. K.; Goodwin, C. A. P.; Chilton, N. F.; Mcinnes, E. J. L.; Winpenny, R. E. P.; Evans, W. J.; Tuna, F. Engineering electronic structure to prolong relaxation times in molecular qubits by minimising orbital angular momentum. *Nat. Commun.* **2019**, *10* (1), No. 3330.

(11) Nodaraki, L. E.; Ariciu, A.-M.; Huh, D. N.; Liu, J.; Martins, D. O. T. A.; Ortu, F.; Winpenny, R. E. P.; Chilton, N. F.; McInnes, E. J. L.; Mills, D. P.; Evans, W. J.; Tuna, F. Ligand Effects on the Spin Relaxation Dynamics and Coherent Manipulation of Organometallic La(II) Potential Qudits. *J. Am. Chem. Soc.* **2024**, *146* (22), 15000−15009.

(12) Kundu, K.; White, J. R. K.; Moehring, S. A.; Yu, J. M.; Ziller, J. W.; Furche, F.; Evans, W. J.; Hill, S. A 9.2-GHz clock transition in a Lu(II) molecular spin qubit arising from a 3,467-MHz hyperfine interaction. *Nat. Chem.* **2022**, *14* (4), 392−397.

(13) Palumbo, C. T.; Zivkovic, I.; Scopelliti, R.; Mazzanti, M. Molecular Complex of Tb in the + 4 Oxidation State. *J. Am. Chem. Soc.* **2019**, *141* (25), 9827−9831.

(14) Rice, N. T.; Popov, I. A.; Russo, D. R.; Bacsa, J.; Batista, E. R.; Yang, P.; Telser, J.; La Pierre, H. S. Design, Isolation, and Spectroscopic Analysis of a Tetravalent Terbium Complex. *J. Am. Chem. Soc.* **2019**, *141* (33), 13222−13233.

(15) Willauer, A. R.; Palumbo, C. T.; Scopelliti, R.; Zivkovic, I.; Douair, I.; Maron, L.; Mazzanti, M. Stabilization of the Oxidation State + IV in Siloxide-Supported Terbium Compounds. *Angew. Chem., Int. Ed.* **2020**, *59* (9), 3549−3553.

(16) Willauer, A. R.; Palumbo, C. T.; Fadaei-Tirani, F.; Zivkovic, I.; Douair, I.; Maron, L.; Mazzanti, M. Accessing the + IV Oxidation State in Molecular Complexes of Praseodymium. *J. Am. Chem. Soc.* **2020**, *142* (12), 5538−5542.

(17) Rice, N. T.; Popov, I. A.; Carlson, R. K.; Greer, S. M.; Boggiano, A. C.; Stein, B. W.; Bacsa, J.; Batista, E. R.; Yang, P.; La Pierre, H. S. Spectroscopic and electrochemical characterization of a Pr^{4+} imidophosphorane complex and the redox chemistry of Nd^{3+} and Dy^{3+} complexes. *Dalton Trans.* **2022**, *51* (17), 6696−6706.

(18) Willauer, A. R.; Douair, I.; Chauvin, A.-S.; Fadaei-Tirani, F.; Bünzli, J.-C. G.; Maron, L.; Mazzanti, M. Structure, reactivity and luminescence studies of triphenylsiloxide complexes of tetravalent lanthanides. *Chem. Sci.* **2022**, *13* (3), 681−691.

(19) Boggiano, A. C.; Chowdhury, S. R.; Roy, M. D.; Bernbeck, M. G.; Greer, S. M.; Vlaisavljevich, B.; La Pierre, H. S. A Four-Coordinate Pr^{4+} Imidophosphorane Complex. *Angew. Chem., Int. Ed.* **2024**, *63* (43), No. e202409789.

(20) Tricoire, M.; Hsueh, F.-C.; Keener, M.; Rajeshkumar, T.; Scopelliti, R.; Zivkovic, I.; Maron, L.; Mazzanti, M. Siloxide tripodal ligands as a scaffold for stabilizing lanthanides in the + 4 oxidation state. *Chem. Sci.* **2024**, *15* (18), 6874−6883.

(21) Xue, T.; Ding, Y.; Zheng, Z. A Tetravalent Praseodymium Complex with Field-Induced Slow Magnetic Relaxation. *Dalton Trans.* **2024**, *53*, 5779−5783.

(22) Boggiano, A. C.; Studvick, C. M.; Roy Chowdhury, S.; Niklas, J. E.; Tateyama, H.; Wu, H.; Leisen, J. E.; Kleemiss, F.; Vlaisavljevich, B.; Popov, I. A.; La Pierre, H. S. Praseodymium in the formal + 5 oxidation state. *Nat. Chem.* **2025**, *17* (7), 1005−1010.

(23) Pandey, P.; Keener, M.; Rajeshkumar, T.; Scopelliti, R.; Sienkiewicz, A.; Zivkovic, I.; Maron, L.; Mazzanti, M. Accessing homoleptic neutral and anionic five-coordinate Pr(IV) siloxide complexes. *Chem. Sci.* **2025**, *16* (44), 21056−21067.

(24) Xue, T.; Yang, Q.-S.; Li, L.; Chang, X.-Y.; Ding, Y.-S.; Zheng, Z. Supramolecular assemblies of tetravalent terbium complex units: syntheses, structure, and materials properties. *Chem. Sci.* **2025**, *16* (16), 6805−6811.

(25) Subintoro, P. J.; Lottes, B.; Pereiro, F. A.; Mahieu, N.; Brown, A. M.; Duggan, S. G.; Mullis, M. S.; Jordan, A. M.; Gates, C.; Greer, S. M.; Woods, J. J.; Abergel, R. J.; Shafer, J. C.; Unruh, D. K.; Miró, P.; Stein, B. W.; Wacker, J. N.; Kozimor, S. A.; Carter, K. P. Structural and spectroscopic characterization of a Tb(IV) polyoxometalate. *Nat. Commun.* **2026**, *17*, No. 8712, DOI: 10.1038/s41467-026-75657-7.

(26) Hu, C.; Demonti, L.; Pandey, P.; Rajeshkumar, T.; Sienkiewicz, A.; Zivkovic, I.; Scopelliti, R.; Maron, L.; Mazzanti, M. Synthesis and Properties of Stable Oxo-Bridged Dinuclear Pr^{IV} Complexes. *J. Am. Chem. Soc.* **2026**, *148* (25), 26698−26709.

(27) Wilkinson, G. R.; Niklas, J. E.; Luevano, M. R.; Nero, T.-R.; Ressnik, F.; La Pierre, H. S. Chapter 354-Molecular Complexes of

Downloaded from pubs.acs.org/inoaj/article-pdf/65/42/25005/6793688/acs.inorgchem.6c04187.pdf by FLORIDA STATE UNIV user on 02 November 2026

High-Oxidation State Lanthanide Ions. In *Handbook on the Physics and Chemistry of Rare Earths*; Bünzli, J.-C. G.; Kauzlarich, S. M., Eds.; Elsevier, 2026; Vol. *69*, pp 131−235.
(28) Daum, M. J.; Ramanathan, A.; Kolesnikov, A. I.; Calder, S.; Mourigal, M.; La Pierre, H. S. Collective excitations in the tetravalent lanthanide honeycomb antiferromagnet Na_2PrO_3. *Phys. Rev. B* **2021**, *103* (12), No. L121109.
(29) Ramanathan, A.; Walter, E. D.; Mourigal, M.; La Pierre, H. S. Increased Crystal Field Drives Intermediate Coupling and Minimizes Decoherence in Tetravalent Praseodymium Qubits. *J. Am. Chem. Soc.* **2023**, *145*, 17603−17612.
(30) Ramanathan, A.; Walter, E. D.; Mourigal, M.; La Pierre, H. S. Correction to "Increased Crystal Field Drives Intermediate Coupling and Minimizes Decoherence in Tetravalent Praseodymium Qubits. *J. Am. Chem. Soc.* **2026**, *148* (28), 30649.
(31) Ramanathan, A.; Kaplan, J.; Sergentu, D.-C.; Branson, J. A.; Ozerov, M.; Kolesnikov, A. I.; Minasian, S. G.; Autschbach, J.; Freeland, J. W.; Jiang, Z.; Mourigal, M.; La Pierre, H. S. Chemical design of electronic and magnetic energy scales of tetravalent praseodymium materials. *Nat. Commun.* **2023**, *14*, No. 3134.
(32) Telser, J. Chapter 3: EPR Interactions - Zero-field Splittings. In *EPR Spectroscopy: Fundamentals and Methods*; Goldfarb, D.; Stoll, S., Eds.; John Wiley & Sons Ltd., 2018.
(33) Goldfarb, D.; Stoll, S. *EPR Spectroscopy: Fundamentals and Methods*; John Wiley & Sons, Ltd., 2018.
(34) Gompa, T. P.; Greer, S. M.; Rice, N. T.; Jiang, N.; Telser, J.; Ozarowski, A.; Stein, B. W.; Pierre, H. S. L. High-Frequency and -Field Electron Paramagnetic Resonance Spectroscopic Analysis of Metal-Ligand Covalency in a $4f^7$ Valence Series (Eu^{2+}, Gd^{3+}, Tb^{4+}). *Inorg. Chem.* **2021**, *60*, 9064−9073.
(35) Ma, C. G.; Brik, M. G.; Li, Q. X.; Tian, Y. Systematic analysis of spectroscopic characteristics of the lanthanide and actinide ions with the $4f^N$ and $5f^N$ (N = 1···14) electronic configurations in a free state. *J. Alloys Compd.* **2014**, *599*, 93−101.
(36) Graham, M. J.; Zadrozny, J. M.; Shiddiq, M.; Anderson, J. S.; Fataftah, M. S.; Hill, S.; Freedman, D. E. Influence of Electronic Spin and Spin−Orbit Coupling on Decoherence in Mononuclear Transition Metal Complexes. *J. Am. Chem. Soc.* **2014**, *136* (21), 7623−7626.
(37) Bader, K.; Winkler, M.; van Slageren, J. Tuning of molecular qubits: very long coherence and spin−lattice relaxation times. *Chem. Commun.* **2016**, *52* (18), 3623−3626.
(38) Graham, M. J.; Krzyaniak, M. D.; Wasielewski, M. R.; Freedman, D. E. Probing Nuclear Spin Effects on Electronic Spin Coherence via EPR Measurements of Vanadium(IV) Complexes. *Inorg. Chem.* **2017**, *56* (14), 8106−8113.
(39) Fataftah, M. S.; Krzyaniak, M. D.; Vlaisavljevich, B.; Wasielewski, M. R.; Zadrozny, J. M.; Freedman, D. E. Metal−ligand covalency enables room temperature molecular qubit candidates. *Chem. Sci.* **2019**, *10* (27), 6707−6714.
(40) Follmer, A. H.; Ribson, R. D.; Oyala, P. H.; Chen, G. Y.; Hadt, R. G. Understanding Covalent versus Spin−Orbit Coupling Contributions to Temperature-Dependent Electron Spin Relaxation in Cupric and Vanadyl Phthalocyanines. *J. Phys. Chem. A* **2020**, *124* (44), 9252−9260.
(41) Mirzoyan, R.; Hadt, R. G. The dynamic ligand field of a molecular qubit: decoherence through spin−phonon coupling. *Phys. Chem. Chem. Phys.* **2020**, *22* (20), 11249−11265.
(42) Jackson, C. E.; Moseley, I. P.; Martinez, R.; Sung, S.; Zadrozny, J. M. A reaction-coordinate perspective of magnetic relaxation. *Chem. Soc. Rev.* **2021**, *50* (12), 6684−6699.
(43) Kazmierczak, N. P.; Mirzoyan, R.; Hadt, R. G. The Impact of Ligand Field Symmetry on Molecular Qubit Coherence. *J. Am. Chem. Soc.* **2021**, *143* (42), 17305−17315.
(44) Mirzoyan, R.; Kazmierczak, N. P.; Hadt, R. G. Deconvolving Contributions to Decoherence in Molecular Electron Spin Qubits: A Dynamic Ligand Field Approach. *Chem.-Eur. J.* **2021**, *27* (37), 9482−9494.
(45) Amdur, M. J.; Mullin, K. R.; Waters, M. J.; Puggioni, D.; Wojnar, M. K.; Gu, M.; Sun, L.; Oyala, P. H.; Rondinelli, J. M.; Freedman, D. E. Chemical control of spin−lattice relaxation to discover a room temperature molecular qubit. *Chem. Sci.* **2022**, *13* (23), 7034−7045.
(46) Kazmierczak, N. P.; Hadt, R. G. Illuminating Ligand Field Contributions to Molecular Qubit Spin Relaxation via T_1 Anisotropy. *J. Am. Chem. Soc.* **2022**, *144* (45), 20804−20814.
(47) Kazmierczak, N. P.; Xia, K. T.; Sutcliffe, E.; Aalto, J. P.; Hadt, R. G. A Spectrochemical Series for Electron Spin Relaxation. *J. Am. Chem. Soc.* **2025**, *147* (3), 2849−2859.
(48) Mariano, L. A.; Nguyen, V. H. A.; Petersen, J. B.; Björnsson, M.; Bendix, J.; Eaton, G. R.; Eaton, S. S.; Lunghi, A. The role of electronic excited states in the spin-lattice relaxation of spin-1/2 molecules. *Sci. Adv.* **2025**, *11* (7), No. eadr0168.
(49) Lunghi, A.Ligand-Field Contributions to Spin-Phonon Coupling in a Family of Vanadium Molecular Qubits from Multi-Reference Electronic Structure Theory. 2019; arXiv:1912.04545. arXiv.org e-Printarchive. https://arxiv.org/abs/1912.04545.
(50) Zsombor-Pindera, J.; Kazmierczak, N.; Mirzoyan, R.; Aalto, J. P.; Kochetov, K.; Fernández, L.; Kiani, P.; Zhou, W.; Hadt, R. G.; Kennepohl, P.Evaluating the Role of Covalency in Spin Relaxation: An XAS Approach. 2026 DOI: 10.26434/chemrxiv-2026-jl6q0.
(51) Kazmierczak, N. P.; Luedecke, K. M.; Gallmeier, E. T.; Hadt, R. G. T_1 Anisotropy Elucidates Spin Relaxation Mechanisms in an S = 1 Cr(IV) Optically Addressable Molecular Qubit. *J. Phys. Chem. Lett.* **2023**, *14* (34), 7658−7664.
(52) Höpfl, H. The tetrahedral character of the boron atom newly defined—a useful tool to evaluate the N→B bond. *J. Organomet. Chem.* **1999**, *581* (1), 129−149.
(53) Cruickshank, P. A. S.; Bolton, D. R.; Robertson, D. A.; Hunter, R. I.; Wylde, R. J.; Smith, G. M. A kilowatt pulsed 94 GHz electron paramagnetic resonance spectrometer with high concentration sensitivity, high instantaneous bandwidth, and low dead time. *Rev. Sci. Instrum.* **2009**, *80* (10), No. 103102.
(54) Subramanya, M. V. H.; Marbey, J.; Kundu, K.; McKay, J. E.; Hill, S. Broadband Fourier-Transform-Detected EPR at W-Band. *Appl. Magn. Reson.* **2023**, *54* (1), 165−181.
(55) Stoll, S.; Schweiger, A. EasySpin, a comprehensive software package for spectral simulation and analysis in EPR. *J. Magn. Reson.* **2006**, *178* (1), 42−55.
(56) Wilson, C. B.; Qi, M.; Han, S.; Sherwin, M. S. Gadolinium Spin Decoherence Mechanisms at High Magnetic Fields. *J. Phys. Chem. Lett.* **2023**, *14* (47), 10578−10584.
(57) Singh, A.; Shrivastava, K. N. Optical-acoustic two-phonon relaxation in spin systems. *Phys. Status Solidi B* **1979**, *95* (1), 273−277.
(58) Shrivastava, K. N. Theory of Spin−Lattice Relaxation. *Phys. Status Solidi B* **1983**, *117* (2), 437−458.
(59) Gu, L.; Wu, R. Origin of the anomalously low Raman exponents in single molecule magnets. *Phys. Rev. B* **2021**, *103* (1), No. 014401, DOI: 10.1103/PhysRevB.103.014401.
(60) Lunghi, A.; Sanvito, S. How do phonons relax molecular spins? *Sci. Adv.* **2019**, *5* (9), No. eaax7163.
(61) Garlatti, E.; Albino, A.; Chicco, S.; Nguyen, V. H. A.; Santanni, F.; Paolasini, L.; Mazzoli, C.; Caciuffo, R.; Totti, F.; Santini, P.; Sessoli, R.; Lunghi, A.; Carretta, S. The critical role of ultra-low-energy vibrations in the relaxation dynamics of molecular qubits. *Nat. Commun.* **2023**, *14* (1), No. 1653, DOI: 10.1038/s41467-023-36852-y.
(62) Kragskow, J. G. C.; Mattioni, A.; Staab, J. K.; Reta, D.; Skelton, J. M.; Chilton, N. F. Spin−phonon coupling and magnetic relaxation in single-molecule magnets. *Chem. Soc. Rev.* **2023**, *52* (14), 4567−4585.
(63) Mondal, S.; Lunghi, A. Spin-phonon decoherence in solid-state paramagnetic defects from first principles. *npj Comput. Mater.* **2023**, *9* (1), No. 120.
(64) Ryan, C.; Lunghi, A.On the Challenge of Simulating Dipolar Contributions to Spin Relaxation with Generalized Cluster

Downloaded from pubs.acs.org/inoca/article-pdf/65/42/25005/6793688/acs.inorgchem.6c04187.pdf by FLORIDA STATE UNIV user on 02 November 2026

Correlation Expansion Methods. 2026; arXiv:2602.14613. arXiv.org e-Printarchive. https://arxiv.org/abs/2602.14613.
(65) Snyder, R. G.; Zerbi, G. Vibrational analysis of ten simple aliphatic ethers: Spectra, assignments, valence force field and molecular conformations. *Spectrochim. Acta, Part A* **1967**, *23* (2), 391−437.
(66) Wieser, H.; Laidlaw, W. G.; Krueger, P. J.; Fuhrer, H. Vibrational spectra and a valence force field for conformers of diethyl ether and deuterated analogues. *Spectrochim. Acta, Part A* **1968**, *24* (8), 1055−1089.

Downloaded from pubs.acs.org/inocaj/article-pdf/65/42/25005/6793688/acs.inorgchem.6c04187.pdf by FLORIDA STATE UNIV user on 02 November 2026

https://doi.org/10.1021/acs.inorgchem.6c04187
Inorg. Chem. 2026, 65, 25005−25013